Universitat Autònoma de Barcelona

Dipòsit digital de documents de la UAB

This is the **submitted version** of the journal article:

Baptista Pires, Luis Miguel; Pérez-López, Briza; Mayorga-Martinez, Carmen C.; [et al.]. «Electrocatalytic tuning of biosensing response through electrostatic or hydrophobic enzyme-graphene oxide interactions». Biosensors and bioelectronics, Vol. 61 (Nov. 2014), p. 655-662. DOI 10.1016/j.bios.2014.05.028

This version is available at https://ddd.uab.cat/record/282554

under the terms of the BY-NC-ND license

Electrocatalytic tune of biosensing response through electrostatic or hydrophobic enzyme – graphene oxide interactions

Luis Baptista-Pires[†], B. Pérez-López [‑], Carmen C. Mayorga-Martinez[†], Eden Morales-Narváez[†] , Neus Domingo[*] , Maria Jose Esplandiu [+] , Francesc Alzina[¥] , C. M. Sotomayor Torres[¥,] and A. Merkoçi [†,*]*

[†] Nanobioelectronics & Biosensors Group, Catalan Institute of Nanoscience and Nanotechnology, ICN2 Campus de la UAB, 08193 Bellaterra, Barcelona, Spain

[‑]LEITAT Technological Center, 08225 Terrasa, Spain

[+] Catalan Institute of Nanoscience and Nanotechnology, ICN2 Campus de la UAB, 08193 Bellaterra, Barcelona, Spain

[*] Oxide Nanoelectronics Group , Catalan Institute of Nanoscience and Nanotechnology, ICN2 Campus de la UAB, 08193 Bellaterra, Barcelona, Spain

[¥] Phononic and Photonic Nanostructures , Catalan Institute of Nanoscience and Nanotechnology, ICN2 Campus de la UAB, 08193 Bellaterra, Barcelona, Spain

[*]ICREA, Institució Catalana de Recerca i Estudis Avançats, 08010 Barcelona, Spain

*corresponding author: Prof. Arben Merkoçi, Phone number: +34935868014; Fax number: +34935868020, E-mail: arben.merkoci@icn.cat

Abstract

The effect of graphene oxidative grades upon the conductivity and hydrophobicity and consequently the influence on an enzymatic biosensing response is presented. The electrochemical responses of reduced graphene oxide (rGO) have been compared with the responses obtained from the oxide form (oGO) and their performances have been accordingly discussed with various evidences obtained by optical techniques. We used tyrosinase enzyme as a proof of concept receptor with interest for phenolic compounds detection through its direct adsorption onto a screen-printed carbon electrode previously modified with oGO or rGO with a carbon - oxygen ratio of 1.07 and 1.53 respectively. Different levels of oGO directly affect the (bio)conjugation properties of the biosensor due to changes at enzyme/graphene oxide interface coming from the various electrostatic or hydrophobic interactions with biomolecules. The developed biosensor was capable to reach a limit of detection of 0.01 nM catechol. This tuning capability of the biosensor response can be with interest for building several other biosensors including immunosensors and DNA sensors with interest for various applications.

Keywords

Oxidized graphene oxide, reduced graphene oxide, electrostatic interactions, hydrophobic interactions, electrocatalytic tune

1. Introduction

Since the discovery of graphene in the last years (Geim and Novoselov 2007) and with the great progress made in nanoscience and nanotechnology, its integration with biomolecules has received increased attention due to its physical, optical and chemical properties such as its interesting molecular structure, high active surface area and high conductivity capacity that improves the electron transfer which are not available in other materials, (Shao et al. 2010). Since then, many graphene materials such as graphene oxide (Marcano et al. 2010; Shen et al. 2009), graphene quantum dots (Peng et al. 2012) or graphene nanoribbons have been reported (Martin-Fernandez et al. 2012).

Graphene oxide (GO) leads to transitions from insulator to semimetallic mainly after reducing processes (Mathkar et al. 2012). The reduction modes such as reduction using hydrazine (Marcano et al. 2010), thermal annealing (Gao et al. 2010) or bacterial treatment (Salas et al. 2010) result in highly reasonable methods for the reconstruction of the carbon sp2 bonds on GO sheets. The reduction of GO removes the oxygen groups and rehybridize the sp^3 carbon atoms to sp^2 carbon atoms (Cheng et al. 2012). Epoxy and hydroxyl groups lie above and below each graphene layer and the carboxylic groups are mostly located at the edges (Zhu et al. 2010). Zhang et al. have demonstrated that reduced graphene oxide (rGO) represent an interesting platform with high affinity for enzyme immobilization. This high affinity is due to the adsorption of enzyme on rGO through hydrophobic interaction and the lack of surface functional groups of rGO that may impart less perturbation to the enzyme (Zhang et al. 2012). Currently different enzymatic biosensors based on

graphene for the detection of different analytes such as that reported by Karuwan et al. (Karuwan et al. 2013) that mixes carbon paste and GO for direct manufacturing of screen printing electrodes, Ping et al. (Ping et al. 2011) that directly electrodeposit GO onto the surface of the electrode and use calcium ion-selective membrane for tuning the biosensor (Ping et al. 2012) have been developed. On the other hand Song et al. (Song et al. 2011) take advantadge of gold nanoparticles, 1-pyrenebutanoic acid and succinimidy ester and Yang et al. (Yang et al. 2013) take advantadge nickel nanoparticles and chitosan.

Due to the biofunctionalization capabilities combined with interesting electrochemical (Shao et al. 2010) and optical properties (Morales-Narvaez and Merkoci 2012) GO has greatly stimulated research interest for applications in (bio)sensing systems. This work presents a new catechol biosensor based on a GO-Tyrosinase conjugate formation through either electrostatic (case of oGO) or hydrophobic (case of rGO) interactions. For this study we have used oGO which have been reduced afterwards with hydrazine (Marcano et al. 2010) so as to achieve its de-oxygenation. The electrochemical responses of this rGO have been compared with the responses obtained for oGO and their performances have been accordingly discussed with various evidences obtained by optical techniques. The use of these GO-based tunning biosystems improves the detection levels comparing with similar technologies (Karuwan et al. 2013; Ping et al. 2011; Ping et al. 2012; Song et al. 2011; Yang et al. 2013) and have advantages of being this a simple technique that doesn't need to use any crosslinking agent, surfactants or other materials as reported before.

2. Materials and methods

2.1 Preparation of rGO. Oxidized graphene oxide (oGO) was provided from Angstron Materials, Inc. (Product: N002-PS) and the reduction step to produce reduced graphene oxide (rGO) was made using reported literature (Marcano et al. 2010) where 100.00 mL of oGO (1mg/mL) was mixed with 1.00 mL of hydrazine hydrate. The mixtures were heated at 95 °C using a water bath for 45 min; a black solid precipitated from the reaction mixture. Products were isolated by filtration (PTFE 20µm pore size) and washed with DI water (50 mL, 3 times) and methanol (20 mL, 3 times).

2.2 Optical measurements and sample characterization. The samples were prepared by drop casting our solution on silicon sample older. X-ray photoelectron spectroscopy (XPS) experiments were performed in a PHI 5500 Multitechnique System (from Physical electronics) with a monochromatic X-ray source (Aluminium Kalfa line of 1486.6 eV energy and 350 W), placed perpendicular to the analyzer axis and calibrated using the 3d5/2 line of Ag with a full width at half maximum (FWHM) of 0.8 eV. Raman spectras were acquired at room temperature with a Horiba T64000 spectrometer operated in single mode configuration with spectral resolution of 4 cm^{-1}. The excitation source was the 514.5 nm line of an argon ion laser. The laser was focused to a spot with diameter of about 560 nm using a 100X objective lens and the intensity was kept below 200µw to avoid any damage of the sample. UV-visible absorbance spectra were explored through SpectraMax $M2^e$ multimode reader (Molecular Devices, California, USA) and fluorescence determined using an UV lamp with 345nm excitation wavelength. AFM

measurements were done using a Dimension 3100 AFM Machine (Veevo metrology group, digital instruments). Easy drop contact angle measuring instrument was used to perform contact angle of modified graphene surfaces.

2.3 SPE modification and electrochemical characterization. SPE were fabricated using a previously optimized technology by our lab. A graphite layer is printed by using the screen-printing machine (DEK 248) with the stencil (where it is the electron pattern) and graphite ink onto the polyester sheet. Polyester sheet is cured during 15 minutes at 95ºC. Silver/silver chloride layer is printed as reference electrode. Polyester sheet is cured during 15 minutes at 95ºC. Insulating ink is deposited. Curing during 20 minutes at 95ºC was performed. SPE were modified with 10µL of 1mg/mL oGO and rGO by drop casting and let dry overnight at room temperature. For exploring electrochemical behavior of modified electrodes, cyclic voltammetry was done using 50µL of 1mM Ferricyanide ($[Fe(CN)_6]^{3-/4-}$) in 1M sodium chloride (KCl) that was deposited onto the SPE by drop casting. Tyrosinase was immobilized onto the electrode surface by physical adsorption. Tyrosinase was solved in 0.1 M phosphate buffer (PBS) at pH 6.5. The concentration of Tyrosinase for SPE modification was 1mg/50µL in PBS. SPE, SPE-oGO and SPE-rGO electrodes have been modified with 5µL of 1mg/50µL Tyrosinase and let it dry overnight in the fridge at 4ºC.

Amperometric measurements were performed applying a potential of -0.1 V in a system composed by a 5 mL electrolytic cell containing 0.1M PBS. PBS is necessary to be used in controlled-potential experiments as a supporting electrolyte. It

decreases the resistance of the solution, eliminates electro migration effects and maintains a constant ionic strength. Cyclic voltammetry (CV) and amperometric experiments were performed using an electrochemical (CH instrument, model CHI 600C).

3. Results and discussion

3.1 optoelectronic properties

X-ray photoelectron spectroscopy (XPS) and Raman spectroscopy (Raman) were firstly used to evidence the level of oxidation and correspondent oxygen bonds so as to determine the structural changes occurring during the chemical reduction process mainly affected by the presence of oxygen atoms onto the graphene structure.

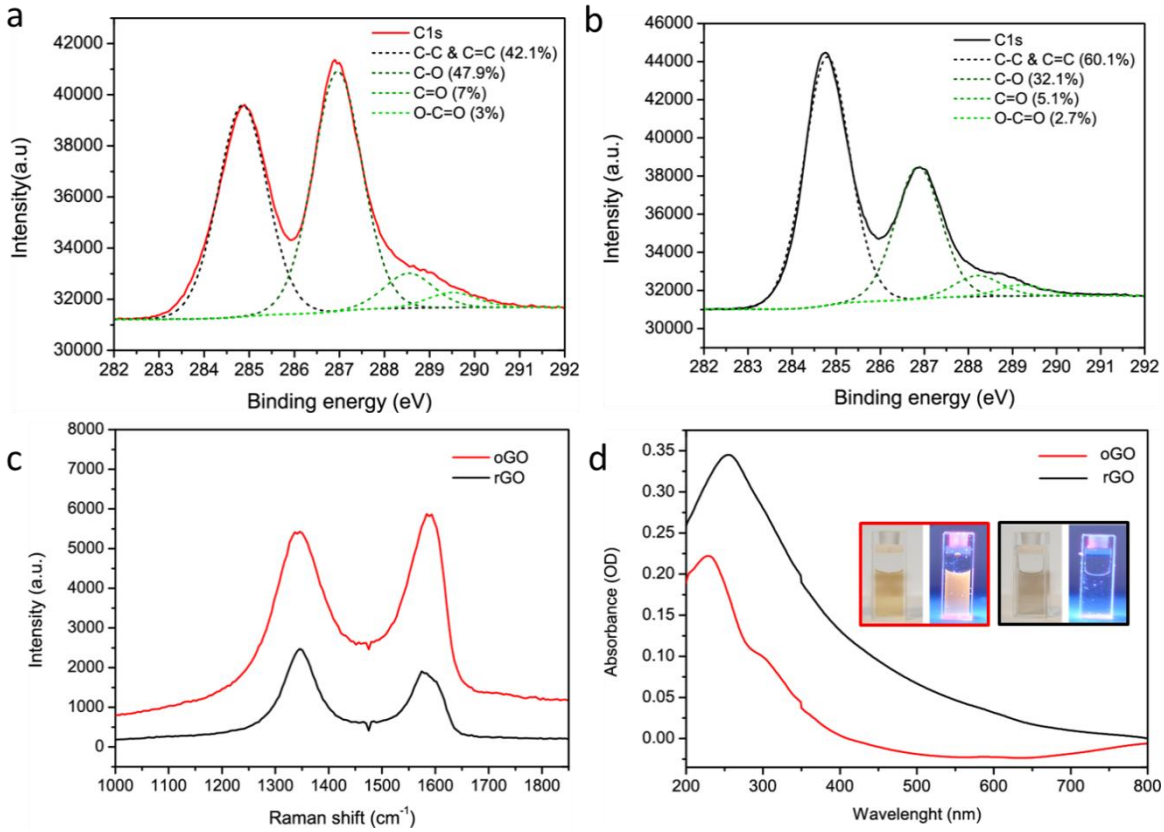

Figure 1. Optical characterization of graphene oxide materials. C1s XPS data of oGO (a) and rGO (b) . (c) Raman spectra and (d) UV-visible steady state spectroscopy. Inset: images of oGO and rGO suspensions under UV lamp excitation.

The study of the efficiency of graphene reduction using hydrazine method was followed by x-ray photoelectron spectroscopy (XPS). Figure 1a shows the C1s signal of oGO powder. The signal was fitted by four components: C=C & C-C (42.1%, 284.6 eV), C-O (47.9%, 286.7 eV), C=O (7%, 288.0 eV) and O=C-OH (3%, 288.9 eV). The estimated ratio C/O is ~1.07. The same study was pursued for rGO represented in Figure 1b with values for C=C & C-C (60.1%, 284.6 eV), C-O (32.1%, 286.7 eV),

C=O (5.1%, 288.0 eV) and O=C-OH (2.7%, 288.9 eV) and a C/O ~1.53. The efficiency of hydrazine reduction is clear and the improvement of the C/O is quantified. In the case of Raman, in Figure 1c the D and G bands are localized at 1345 cm^{-1} and 1590 cm^{-1} respectively for oGo and rGO (Park et al. 2008a). However, an increase in D/G intensity ratio (I_D/I_G) is observed for rGO (I_D/I_G = 1.26) in comparison with oGO (I_D/I_G = 0.92) suggesting a decrease in the average size of the sp^2 domains upon reduction and can be explained by the formation of new graphitic domains that are smaller in size but more numerous (Stankovich et al. 2007). According to this study, the modified screen printing electrodes (SPE) with these two kinds of graphene, possess levels of oxidation and carbon networks completely different, and consequently different electrocatalytic responses can be previewed. In order to get insights of the electronic properties of the obtained platform, UV-Visible spectrum was performed and is represented on Figure 1d. For the oGO sample, a maximum peak at 231 nm is ascribed to π→π* transition of aromatic C–C bonds, and a shoulder at 300 nm is attributed to *n*→π* transition of C=O bonds. In the case of the rGO, the maximum peak was red-shifted to 254 nm after reduction and the absorbance was significantly increased at wavelengths above 233 nm, which indicates that electronic conjugation has been restored, at least to some extent(Cuong et al. 2010). The defect at 350 nm on the visible spectra is due to the UV lamp change on the device. The fact that under excitation of 350nm UV-light, the oGO presents fluorescence (inset Figure 1d) in detriment of rGO can make us think about the transitions presented on the UV-Visible absorbance spectra which are in line with similar data of an oxidized graphene material (Shang et al. 2012) for which the appearance of a band gap has been also reported.

3.2 Morphology characterization

To accurately determine the oGO and rGO morphology at the nanoscale, the sheets were characterized by Atomic Force Microscopy (AFM), as shown in Figure 2.

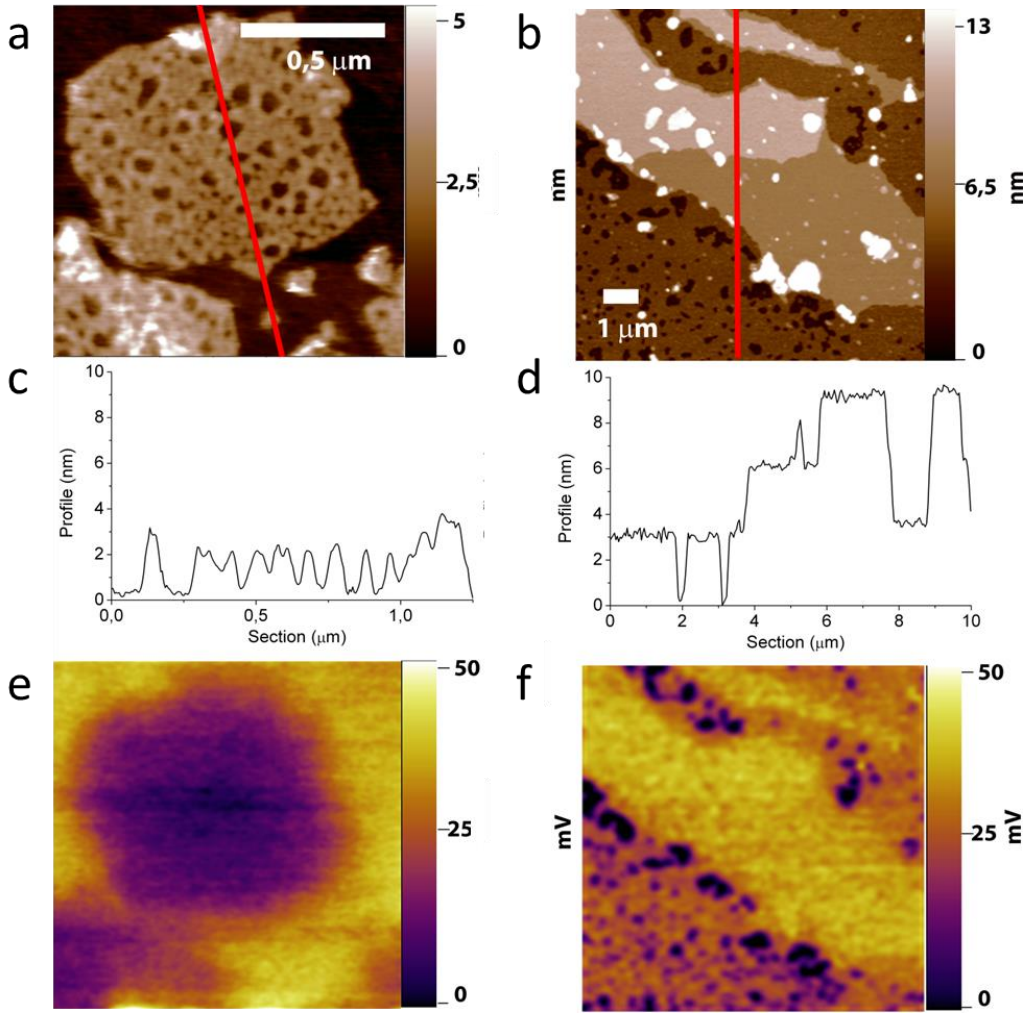

Figure 2. Graphene oxide morphology at the nanoscale. Topography AFM images of oGO (a) and rGO (b) flakes. The red lines correspond to the sections (c) and (d) shown below for each image. KPFM images of oGO (e) and rGO (f) of the same area as (a) and (b).

Completely different morphologies were observed between these two nanomaterials. oGO flakes show a high non-uniform surface with high degree of porosity. The average diameter of graphene holes is in the range of tens of nanometers, and the flakes show a thickness of about 2.5 nm. The presence of this topographical defects observed in this sample is explained by the high level of oxidation(Cheng et al. 2012). Indeed, Figure 2b shows the topography of rGO flakes in which homogeneous double, triple and multilayer flakes of graphene are observed(Geim and Novoselov 2007). The average thickness of each flake for this sample is around 3 nm. It becomes clear that the reduction process of oGO flakes results onto bigger layers of rGO after reduction of oGO, mostly due to the rearrangement of sp^2 carbon bonds (Gao et al. 2010).

The different levels of oxidation of the oGO and rGO films are confirmed by Kelvin Probe Force Microscopy (KPFM) and surface hydrophobicity studies. In KPFM, the direct measurements of the contact potential difference between the oGO and rGO flakes and the tip of the AFM are obtained and mapped. As shown in Figure 2c and 2d, the KPFM image of the oGO flakes shows a dark contrast with respect to the surrounding substrate, indicating the presence of negative dipoles on the surface of the oGO flakes dominated by the oxygen groups. Instead, for rGO, the flakes show a more positive contrast with respect to the substrate observed through the holes, in agreement with the presence of less negative dipoles on the surface of these samples which are arisen from the reconstruction of the sp^2 carbon network.

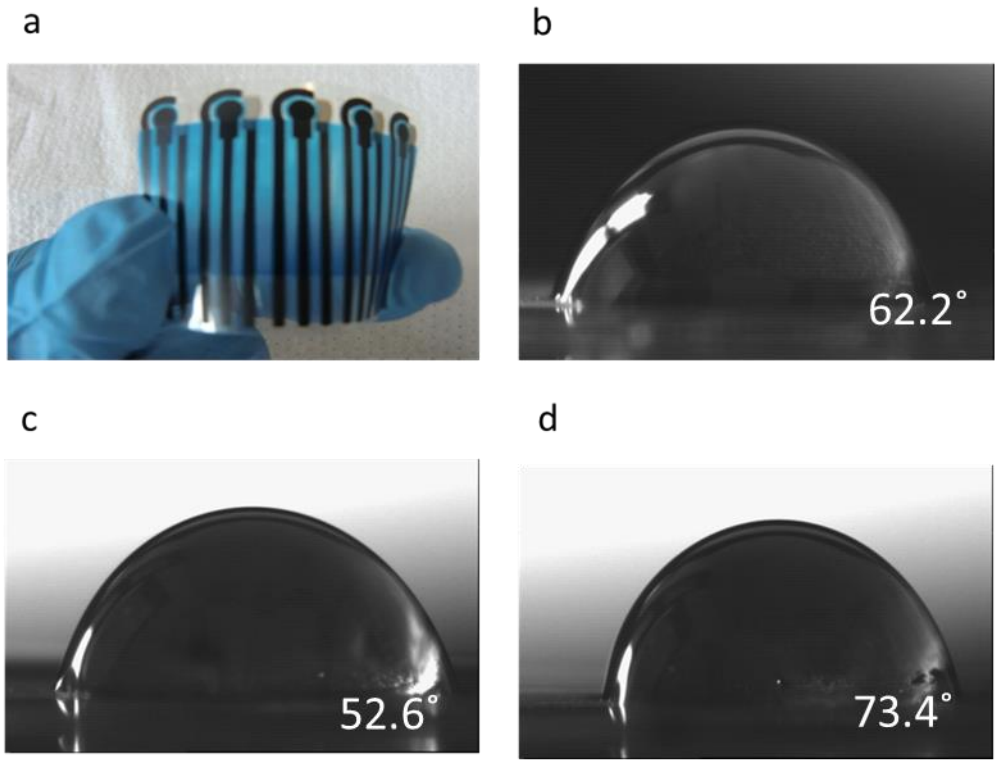

Figure 3. Surface hydrophobicity study. SPE flexible technology (a). Water contact angles for SPE (b), SPE-oGO (c) and SPE-rGO (d).

In order to evaluate the surface hydrophobicity and the electrocatalytic properties of the graphene forms we used SPE (Figure 3a) as testing platforms. Screen-printing microfabrication technology is well-established for the mass production of thick film electrodes and it is widely applied to build biological or chemical sensors(Fanjul-Bolado et al. 2009). SPE represents one of the most important products of this technology.. A simple strategy in which SPE`s were modified with 10µL of 1mg/mL

oGO and rGO was used. Under this methodology a total coverage of the SPE is achieved and a completely new electrode platform is built.

Surface hydrophobicity of the modified SPE was evaluated due to the fact that adsorption processes have a direct influence on the electrochemical response through the electrocatalytic behavior of the adsorbed enzyme. As shown in Figure 3b, the contact angle to water of typical SPE is 62.2˚. After modification with graphene oxide materials, the surface suffers visible changes on its hydrophobicity. In the case of SPE modified with oGO (SPE-oGO) in Figure 3c, the surface changed to a value of 52.6˚ and in the SPE modified with rGO (SPE-rGO) the contact angle was 73.4˚ as reported in Figure 3d. (Zhang et al. 2012). In the case of SPE-oGO the surface seems to be much more hydrophilic in comparison with SPE-rGO due to the presence of oxide groups. The consequent removal of these oxygen binding sites for rGO-SPE induced stronger hydrophobicity on these electrodes due to π-π interactions. These results are also in agreement with the level of oxidation of the graphene materials that is proportional to the hydrophobicity of the modified SPE surface and consistent with the AFM measurements.

3.3 Electrocatalytic properties

To explore electrocatalytic behavior of the modified SPE electrodes, a drop of 50μL of 1mM Ferricyanide ($[Fe(CN)_6]^{3-/4-}$) solution was deposited and cyclic voltammetry technique was performed to evaluate electrochemical response of SPE-oGO and SPE-rGO to this redox couple.

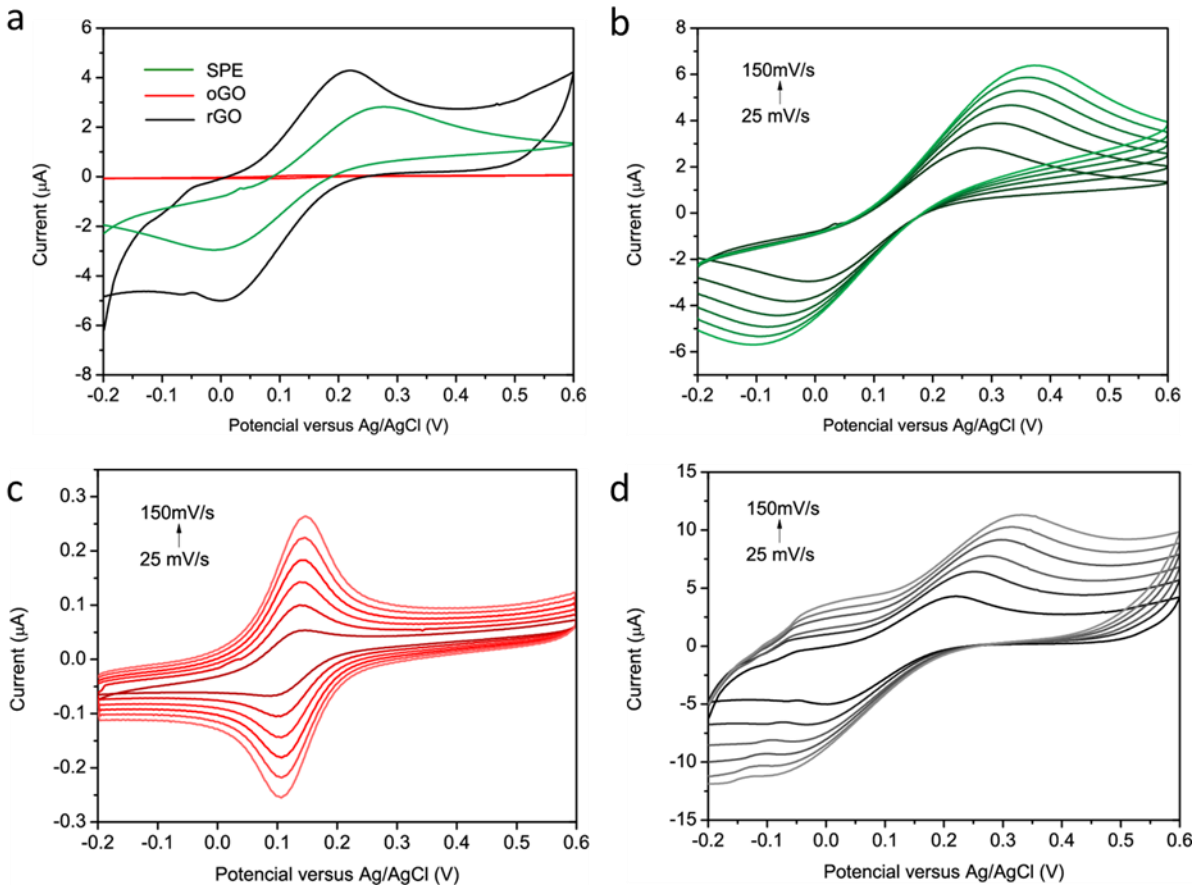

Figure 4. Electrochemical properties. Cyclic voltammetry for SPE, SPE-oGO and SPE-rGO at a scan rate of 25mV/s (a). Non-modified SPE (b), SPE-oGO (c) and SPE-rGO (d) at scan rates from 25mV/s to 150mV/s. All samples were tested in 1mM $[Fe(CN)_6]^{3-/4-}$ in 1M KCl.

Figure 4 shows that the presence of graphene materials has an important effect on the electrochemical response of the SPEs. While the presence of oGO decreases the conductivity or the current on the SPE-oGO, the SPE-rGO shows a higher

current response to $[Fe(CN)_6]^{3-/4-}$ (Figure 4a). From these results, one can state than rGO is the most conductive material and oGO the most resistive one. As a matter of comparison, the electrochemical behavior of the SPE electrode without graphene (Figure 4b) together with a zoom of the electrochemical response of the SPE-oGO (Figure 4c) and SPE-rGO (Figure 4d) is also depicted. In the SPE-oGO a very low current redox wave whose possible origin will be addressed later on was also captured.

The electrochemical reactivity of the SPE-oGO and SPE-rGO can be explained under the light of the density of electronic states which is a very important parameter that controls the electrode kinetics. According to Gerischer-Marcus theory, the heterogeneous electron transfer rate is dependent on DOS of the electrode and on their overlap with the electronic states of the electroactive species (Belding et al. 2010). An electron transfer can take place from any occupied energy state that is matched in energy with an occupied receiving state. Thus in metallic electrodes the high density of DOS increases the possibility that an electron of the correct energy is available for the electrode to transfer to an electroactive species. However if the material exhibits a band gap the probability of matching available states for the electron exchange between electrode and electroactive species is very low decreasing dramatically the electrochemical activity. Therefore in the case of SPE-oGO and in accordance with the fluorescence observations, it is very reasonable to ascribe the low electrochemical performance to the opening of band gap with the oxidation process.

High graphene oxidation is known for instance to remove states close to the Fermi level, thus producing an insulator (Acik et al. 2010). It is therefore expected that excessive oxygen moieties on graphene in any chemical form (epoxide, hydroxyl, carboxyl and ketonic-type functional groups) both on the basal plane (Cai et al. 2008) and at the edges(Park et al. 2008b) reduces electronic states at the Fermi level and consequently its conductivity as probed experimentally (Eda et al. 2009). As described before in Figure 1d, the reduction of oGO results on the decrease of $n \rightarrow \pi^*$ transitions, responsible for C=O bonds in sp^3 hybrid regions and responsible for fluorescence emission in graphene oxide (Shang et al. 2012). It is also reported that graphene reduction using hydrazine decreases the band gap to values almost negligible (Mathkar et al. 2012). The conductivity increase after reduction, passing from an insulator material to a more semimetallic conductive one is clear in Figure 4d and consistent with literature reported elsewhere about this transition behavior upon reduction (Acik et al. 2010).

Table 1. Cyclic Voltammetry data for SPE, SPE-CGO and SPE-RGO

	ΔE(V)	ΔI(μA)
SPE	0.3945	4.72
PE-CGO	0.0244	0.12
SPE-RGO	0.3297	7.75

Redox peak currents increase around sixty times upon reduction as can be observed in Table 1. The table also reports the peak separation voltages (ΔV_p) for the different electrodes. It can be observed that the ΔV_p of SPE-rGO is smaller than in the case of the carbon based SPE evidencing the favourable electrode kinetics of the reduced graphene. The table also reports the ΔV_p value for the case of SPE-oGO ascribed to the very low current oxidation/reduction wave which is captured when zooming in the electrochemical current of the oxidized graphene. The origin of such small redox wave and its surprising low value of ΔV_p cannot be analyzed in the same context as in the case of SPE and SPE-rGO electrodes. We believe that such redox wave in the SPE-oGO is coming from the response of the bottom carbon support of the SPE and not from the oxidized and insulating graphene. The surprising reversibility of such wave can be explained under the light of the thin layer diffusion model which is applicable when the electrolyte is trapped in porous layers(Belding et al. 2010). Indeed, AFM images have shown the porous nature of oxidized graphene. Therefore the electrochemical response is compatible with a passivating oxidized graphene layer with a number of pits (pores) through which the electrolyte penetrates and keeps confined, inducing a kinetically and thermodynamically favourable electron transfer with the base carbon material of the SPE. Accordingly, the peak-to-peak separation in this scenario is expected to be smaller than in the case of the semi-infinite diffusion model in agreement with our findings.

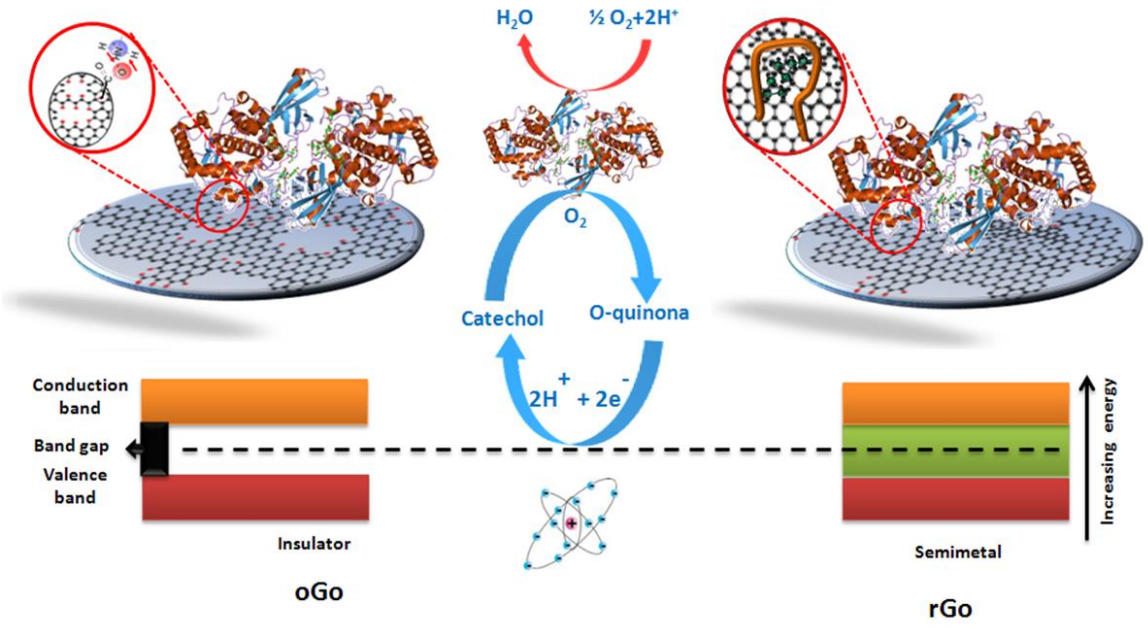

Figure 5: Schematic diagram (not in scale) displaying the enzyme (Tyrosinase) and reactions involved in the catechol detection at the SPE modified with oGO acting as an insulator and rGO as a semimettalic compound.

The influence of the two explored graphene materials with different levels of oxidation on the attachment of Tyrosinase enzyme has been also studied. The enzymatic activity of the Tyrosinase-graphene oxide modified SPE platform using catechol can be observed through the formation of *o*-Quinone as shown in Figure 5.

The voltamperometric evaluation (Figure 6a) shows the comparison of the SPE modified with Tyrosinase (SPE/Tyr), oGO plus tyrosinase (SPE/oGO/Tyr) and rGO plus tyrosinase on the electrocatalytic detection of catechol. All modifications and measurements with the developed biosensors were done under strictly identical

conditions (the total assay time including the SPE modifications through incubations with graphene was around 24 hours). As expected, the reduction signal was improved when GO was present. Moreover, remarkably higher response of SPE/rGO/Tyr was observed, showing fairly well the advantages predicted for this type of biosensor configuration, commented in the introduction section. The enzymatic reaction involves the catalytic oxidation of the catechol to o-quinones, at the expense of reducing oxygen to water. The electrochemical reduction of o-quinones, by transferring two electrons and two protons, was employed to monitor this reaction (Fig. 5). In this case, o-quinone can be reduced back to catechol at low applied potentials (-0.1V). The generation of electrons in this step leads to a change in the current that can be measured. The coupling between the catalytic oxidation (catechol to *o*-quinone) and the electrochemical reduction (*o*-quinone to catechol) shuttles the catechol into a cycle with the possibility of signaling amplification (see Figure 6b).

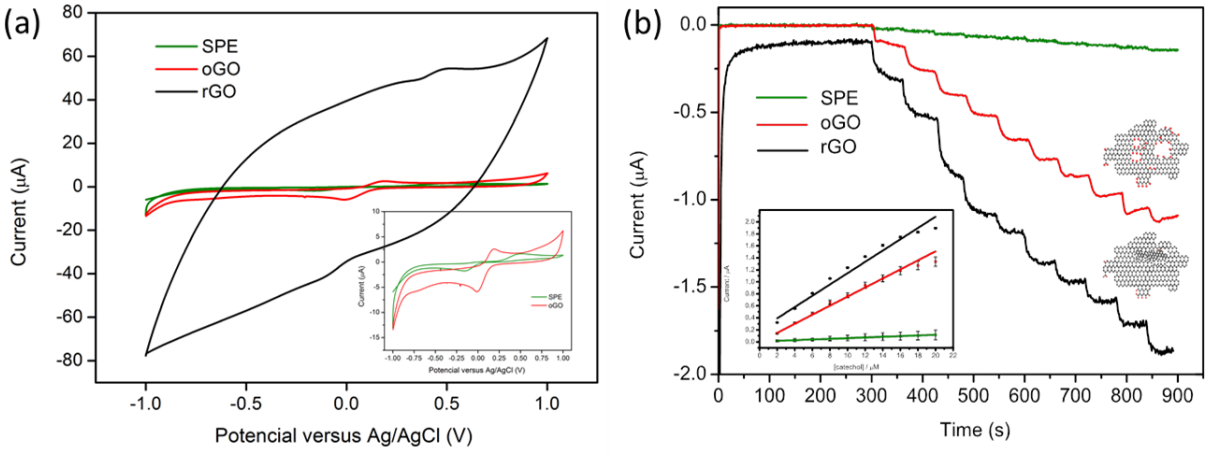

Figure 6. Electrocatalytic properties of SPE/Tyr, SPE/oGO/Tyr and SPE/rGO/Tyr. (a) Cyclic voltammetry response in presence of 20 μM Catechol at 100 mVs^{-1}. (b) Typical current-time curves for the successive additions of 2 μM catechol solution, to a 5mL electrocatalytic cell containing 0.1M PBS (pH 6.5) during stirring conditions under a working potential of -0.1V. Inset: corresponding calibration curves for the graphene modified SPEs.

Herein SPE, SPE-oGO and SPE-rGO electrodes have been modified with Tyrosinase by adsorption. Such immobilization strategy and the final enzymatic activity are expected to be very dependent on the hydrophobicity level of the GO-SPE. The enzymatic response has been followed up by amperometric measurements at -0.1 V. We have found a very good electrochemical stability to the addition of catechol for the highly oxidized graphene as can be observed in Figure 6b. This behavior may be related with the binding of the Tyr to oGO by electrostatic interaction (Zhang et al. 2012). Thus and despite being an insulator, SPE-oGO results highly beneficial for enzyme biosensing platforms presenting a limit of detection (LOD – signal to noise ratio (S/N) = 3)) of 0.0711nM, a limit of quantification (LOQ) of 0.237nM and a sensitivity of 0.0679μA/μM as presented on table 2. In the case of SPE-rGO modified with Tyr, the improvement of the electroanalytical performance (based on LOD and sensitivity parameters) was observed. The presence of hydrophobic aromatic structures observed by XPS spectra (Fig. 1b) and the water contact angles studies (Fig. 3d) suggested that the adsorption of the enzyme onto SPE-rGO should be government by a hydrophobic interaction instead

of electrostatic interaction as onto SPE-oGO. As reported before, this Tyrosine immobilization onto the rGO was more efficient than the immobilization onto the oGO for similar C/O (Zhang et al. 2012). This phenomenon is attributed to the fact that the electrostatic interaction as the driving force for enzyme binding to oGO severely affected the activity of the enzyme. Additionally the higher conductivity of the rGO promotes high charge transfer (Fig. 4a). As reported in table 2, the SPE-rGO presented the best LOD of all graphene materials (0.0103nM), a LOQ of 0.034nM and was shown to be the most sensitive (0.0898µA/µM).

Table 2. Description of different analytical parameters

	LOQ (nM)	LOD (nM)	Sensitivity ($\mu A \cdot \mu M^{-1}$)	Linear Interval (µM)	R^2
SPE	1.379	0.4140	0.0056	2-16	0.9936
SPE-CGO	0.237	0.0711	0.0679	2-16	0.9954
SPE-RGO	0.034	0.0103	0.0898	2-16	0.9918

The obtained results are advantageous when concerning biosensors reported in literature (Karuwan et al. 2013; Ping et al. 2011; Ping et al. 2012; Song et al. 2011; Yang et al. 2013) that use other nanomaterials or a cross-linked agent and longer procedures to immobilize the enzymes and enhance the response. The proposed graphene-based biosensing fabrication is simple, time efficient and doesn't alter the enzyme structure and its operation yielding very good performance.

4. Conclusions

As experimentally observed in this work, graphene materials where deeply characterized in terms of morphology and optoelectronic properties. The electrochemical behavior upon the addition of GO over a screen-printed electrode in terms of current responses is described. In addition, it is demonstrated that the biofuncionalization capability might have been affected by the level of oxidation of graphene materials (oGO with a C/O of 1.07 and rGO with a C/O of 1.53). These different C/O levels should have contributed in the biosensor performance (better stability due to a better enzyme immobilization onto SPE modified with rGO by hydrophobic interaction) and the decrease of the limit of detection in comparison to the non-modified SPE and the SPE modified with oGO. The results show that the SPE modification with oGO leads to low level tyrosinase biofunctionality (although much higher than the SPE without oGO) while the modification with highly hydrophobic and conductive rGO leads to a higher level of biofuncionalization. This tuning capability of the biosensor response can be with interest for building several other biosensors including immunosensors and DNA sensors with interest for various applications.

5. Acknowledgments

MEC (Spain) for MAT2011-25870 grant is acknowledged. The technical support on graphene oxide characterization given by Pablo Garcia, Marcos Rosado, Guillaume Saufier and Javier Saiz Poseu from Institut Catalá de Nanosciencia I Nanotecnologia (ICN2) is also acknowledged.

6. References

Acik, M., Lee, G., Mattevi, C., Chhowalla, M., Cho, K., Chabal, Y.J., 2010. Nat. Mater. 9(10), 840-845.

Belding, S.R., Campbell, F.W., Dickinson, E.J.F., Compton, R.G., 2010. Phys. Chem. Chem. Phys. 12(37), 11208-11221.

Cai, W.W., Piner, R.D., Stadermann, F.J., Park, S., Shaibat, M.A., Ishii, Y., Yang, D.X., Velamakanni, A., An, S.J., Stoller, M., An, J.H., Chen, D.M., Ruoff, R.S., 2008. Science 321(5897), 1815-1817.

Cheng, M., Yang, R., Zhang, L.C., Shi, Z.W., Yang, W., Wang, D.M., Xie, G.B., Shi, D.X., Zhang, G.Y., 2012. Carbon 50(7), 2581-2587.

Cuong, T.V., Pham, V.H., Tran, Q.T., Hahn, S.H., Chung, J.S., Shin, E.W., Kim, E.J., 2010. Mater. Lett. 64(3), 399-401.

Eda, G., Mattevi, C., Yamaguchi, H., Kim, H., Chhowalla, M., 2009. J. Phys. Chem. C 113(35), 15768-15771.

Fanjul-Bolado, P., Lamas-Ardisana, P.J., Hernandez-Santos, D., Costa-Garcia, A., 2009. Anal. Chim. Acta 638(2), 133-138.

Gao, X.F., Jang, J., Nagase, S., 2010. J. Phys. Chem. C 114(2), 832-842.

Geim, A.K., Novoselov, K.S., 2007. Nat. Mater. 6(3), 183-191.

Karuwan, C., Wisitsoraat, A., Phokharatkul, D., Sriprachuabwong, C., Lomas, T., Nacapricha, D., Tuantranont, A., 2013. Rsc Advances 3(48), 25792-25799.

Marcano, D.C., Kosynkin, D.V., Berlin, J.M., Sinitskii, A., Sun, Z.Z., Slesarev, A., Alemany, L.B., Lu, W., Tour, J.M., 2010. Acs Nano 4(8), 4806-4814.

Martin-Fernandez, I., Wang, D.B., Zhang, Y.G., 2012. Nano Lett. 12(12), 6175-6179.

Mathkar, A., Tozier, D., Cox, P., Ong, P.J., Galande, C., Balakrishnan, K., Reddy, A.L.M., Ajayan, P.M., 2012. J. Phys. Chem. Lett. 3(8), 986-991.

Morales-Narvaez, E., Merkoci, A., 2012. 24(25), 3298-3308.

Park, S., An, J.H., Piner, R.D., Jung, I., Yang, D.X., Velamakanni, A., Nguyen, S.T., Ruoff, R.S., 2008a. Chem. Mat. 20(21), 6592-6594.

Park, S., Lee, K.S., Bozoklu, G., Cai, W., Nguyen, S.T., Ruoff, R.S., 2008b. ACS Nano 2(3), 572-578.

Peng, J., Gao, W., Gupta, B.K., Liu, Z., Romero-Aburto, R., Ge, L.H., Song, L., Alemany, L.B., Zhan, X.B., Gao, G.H., Vithayathil, S.A., Kaipparettu, B.A., Marti, A.A., Hayashi, T., Zhu, J.J., Ajayan, P.M., 2012. Nano Lett. 12(2), 844-849.

Ping, J., Wang, Y., Fan, K., Wu, J., Ying, Y., 2011. Biosensors & Bioelectronics 28(1), 204-209.

Ping, J., Wang, Y., Ying, Y., Wu, J., 2012. Anal. Chem. 84(7), 3473-3479.

Salas, E.C., Sun, Z.Z., Luttge, A., Tour, J.M., 2010. ACS Nano 4(8), 4852-4856.

Shang, J.Z., Ma, L., Li, J.W., Ai, W., Yu, T., Gurzadyan, G.G., 2012. Sci Rep 2.

Shao, Y.Y., Wang, J., Wu, H., Liu, J., Aksay, I.A., Lin, Y.H., 2010. Electroanalysis 22(10), 1027-1036.

Shen, J.F., Hu, Y.Z., Shi, M., Lu, X., Qin, C., Li, C., Ye, M.X., 2009. Chem. Mat. 21(15), 3514-3520.

Song, W., Li, D.-W., Li, Y.-T., Li, Y., Long, Y.-T., 2011. Biosensors & Bioelectronics 26(7), 3181-3186.

Stankovich, S., Dikin, D.A., Piner, R.D., Kohlhaas, K.A., Kleinhammes, A., Jia, Y., Wu, Y., Nguyen, S.T., Ruoff, R.S., 2007. Carbon 45(7), 1558-1565.

Yang, J., Yu, J.-H., Strickler, J.R., Chang, W.-J., Gunasekaran, S., 2013. Biosensors & Bioelectronics 47, 530-538.

Zhang, Y., Zhang, J.Y., Huang, X.L., Zhou, X.J., Wu, H.X., Guo, S.W., 2012. Small 8(1), 154-159.

Zhu, Y.W., Murali, S., Cai, W.W., Li, X.S., Suk, J.W., Potts, J.R., Ruoff, R.S., 2010. Adv. Mater. 22(35), 3906-3924.